Calculation of the near fields for the scattering of electromagnetic waves by multiple infinite cylinders at perpendicular incidence

J. Schäfer[a,*], S.-C. Lee[b], A. Kienle[a]

[a] *Institut für Lasertechnologien in der Medizin und Meßtechnik an der Universität Ulm, Helmholtzstr. 12, 89081 Ulm, Germany*
[b] *Applied Sciences Laboratory, Inc., Baldwin Park, California 91706, USA*

Abstract

The near field solution for the scattering of a plane monochromatic electromagnetic wave by an ensemble of parallel infinite dielectric cylinders at perpendicular incidence is presented in this paper. The solution is given for the calculation of the electric and magnetic near fields and the Poynting vector. A MATLAB program has been developed to solve the near field formulas which is introduced and validated. The near to far field transition as well as formation and transport of photonic nanojets have been calculated for multiple cylinder scattering.

Keywords: Electromagnetic scattering, Near field solution, Dependent scattering, Infinite cylinder, Photonic nanojet, Finite difference time domain method

1. Introduction

The theoretical investigation of electromagnetic scattering by small particles is of severe interest in different research fields, e.g. remote sensing, heat transfer or light propagation in biological tissue [1]. Though the experimentally measured scattering samples are usually of complex shape and composition, much knowledge of scattering processes can be gained by looking at the theoretical scattering solutions for simplified geometries. For the theoretical examination of many problems, e.g. the scattering of light by cells in tissue [2] or the study of radiative properties of aerosols in atmosphere [3], spherical scatterers can be applied as simple models. The solution of the scattering of electromagnetic waves by a sphere (Mie theory) [4] and their extensions, e.g. the scattering by a layered sphere [5], the multiple scattering Mie solution (GMM) [6] or the generalized Lorenz-Mie theory for an incident Gaussian beam (GLMT) [7], are widely used for this purpose.

Another fundamental scattering structure for which an analytical solution has been developed is the infinite cylinder [1]. For many scattering problems, e.g. thermal radiation

*Corresponding Author. Tel.:+497311429229;fax:+497311429442.
Email address: jan.schaefer@ilm.uni-ulm.de (J. Schäfer)

in fibrous materials [8] or light propagation in anisotropic biological media like skin, muscle or tooth [9], cylindrical structures can be identified as primal scattering objects. If the length of the cylindrical scattering structures is much larger than the diameter, the infinite cylinder approximation can be applied [10], which is e.g. the case for human dentin [9]. Analogous to the Mie solution, a various number of extensions exists for the infinite cylinder scattering theory, which include layered particle [5, 11], multiple particles [12, 13, 14] and Gaussian beam solutions [15].

In most electromagnetic scattering applications, the scattered field is measured in a certain distance to the scattering structure, which is in the far field. Therefore, in theoretical investigations often merely the far field solutions of the scattering problems are regarded. However, the basis of the Mie and cylinder theories is actually located in the near fields. The far field solution can be obtained by limiting value considerations of the near field formulas. Apart from the far field solution also the near field solution can play an important role in improving the understanding of the scattering of electromagnetic waves by small particles. Many interesting phenomena, like photonic nanojets [16] or local field enhancement [17], can only be described by considering the near field solutions.

In this paper the near field solution for the light scattering by multiple parallel infinite cylinders at perpendicular incidence is presented. In the first section the theoretical derivation of the solution is sketched and the relevant formulas are summarized. The next section shows validation results for the numerical calculation of the analytical solution in comparison to numerical results obtained with the finite difference time domain (FDTD) method [18]. The implemented formulas have been utilized to examine the near to far field transition for the scattering by multiple cylindrical particles which is detailed in the subsequent section. In addition the transport of energy of a photonic nanojet through a multiparticle system has been investigated. In the last section some concluding remarks are appended.

2. Theory

In this section the near field solution for the scattering of a monochromatic plane electromagnetic wave by an ensemble of parallel infinite cylinders at perpendicular incidence is presented. The solution is based on the multiple cylinder scattering formalism of Lee [13], another solution has been presented by Henin et al. [19]. The cylinders do not overlap but can have different optical properties and radii. In an ensemble of N particles the radius of each cylinder $i \in \{1 \dots N\}$ is defined as a_i, the complex refractive index inside the cylinder is given by n_i. The cylinders are embedded in a non-absorbing outer medium with real refractive index n_m and illuminated by a plane electromagnetic wave with vacuum wave number k_0. The wave number inside the outer medium is given by $k_m = k_0 n_m$, the wave number inside each particle by $k_i = k_0 n_i$. In figure 1 a scheme of a two-particle scattering problem is shown. The plane wave is incident at an angle φ_i relative to the x-axis, the cylinder axes are aligned parallel to the z-axis. The cylinders are placed at points P_i, the near field is considered at point $P = P(\rho, \phi)$. R_{iP} is the distance between point P_i and point P. The angle between the positive x-axis and the connection line $\vec{R}_{iP} = \overline{P_i P}$ is defined as γ_{iP}. R_{jl} is the distance between two cylinders j, l, the angle between the connection line $\vec{R}_{jl} = \overline{P_j P_l}$ and the x-axis is defined by γ_{jl}.

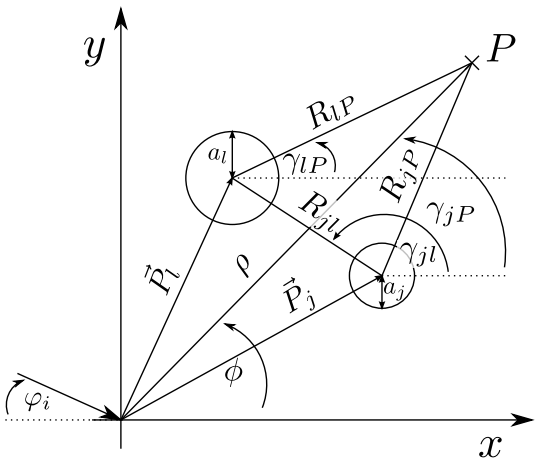

Figure 1: Definition of the distance and angle parameters used for the solution of the multiple cylinder scattering.

2.1. Hertz potentials

In a homogeneous medium with refractive index n the complete field solution of the scattering problem ($\vec{E}$, $\vec{H}$) can be expressed in terms of two scalar Hertz potentials (u, v) [11]. These Hertz potentials have to satisfy the wave equation:

$$\left(\Delta + (nk_0)^2\right) \cdot \begin{bmatrix} u \\ v \end{bmatrix} = 0. \tag{1}$$

With known potentials the field solution inside a homogeneous medium is given as follows [11]:

$$\vec{E} = \frac{i}{nk_0} \nabla \times \nabla \times \vec{u} + \nabla \times \vec{v}, \tag{2a}$$

$$\vec{H} = -n \nabla \times \vec{u} + \frac{i}{k_0} \nabla \times \nabla \times \vec{v}, \tag{2b}$$

$$\vec{u} = (0, 0, u)^T, \tag{3a}$$

$$\vec{v} = (0, 0, v)^T. \tag{3b}$$

For the case of infinite cylinders it is appropriate to formulate the problem in cylindrical coordinates. Due to symmetry along the axis of infinity (z-axis) the z-derivatives vanish

and the field solution in cylindrical coordinates can be expressed as

$$E_\rho = \frac{1}{\rho}\frac{\partial v}{\partial \phi}, \quad (4a) \qquad H_\rho = -\frac{n}{\rho}\frac{\partial u}{\partial \phi}, \quad (4b)$$

$$E_\phi = -\frac{\partial v}{\partial \rho}, \quad (4c) \qquad H_\phi = n\frac{\partial u}{\partial \rho}, \quad (4d)$$

$$E_z = -\frac{i}{nk_0}\left[\frac{1}{\rho}\frac{\partial}{\partial \rho}\rho\frac{\partial}{\partial \rho} + \frac{1}{\rho^2}\left(\frac{\partial}{\partial \phi}\right)^2\right]u, \quad (4e) \qquad H_z = -\frac{i}{k_0}\left[\frac{1}{\rho}\frac{\partial}{\partial \rho}\rho\frac{\partial}{\partial \rho} + \frac{1}{\rho^2}\left(\frac{\partial}{\partial \phi}\right)^2\right]v. \quad (4f)$$

The field solution splits up into two independent solutions, the transverse magnetic mode (TM, u) and the transverse electric mode (TE, v), respectively.

The incident field for both modes is given by the following equations:

$$\vec{E}^0_{\mathrm{TM}} = ik_m e^{-ik_m(x\cos\varphi_i - y\sin\varphi_i)}\hat{e}_z, \quad (5a)$$

$$\vec{H}^0_{\mathrm{TM}} = -ik_m n_m e^{-ik_m(x\cos\varphi_i - y\sin\varphi_i)}\left(\sin\varphi_i\hat{e}_x + \cos\varphi_i\hat{e}_y\right), \quad (5b)$$

$$\vec{E}^0_{\mathrm{TE}} = ik_m e^{-ik_m(x\cos\varphi_i - y\sin\varphi_i)}\left(\sin\varphi_i\hat{e}_x + \cos\varphi_i\hat{e}_y\right), \quad (5c)$$

$$\vec{H}^0_{\mathrm{TE}} = ik_m n_m e^{-ik_m(x\cos\varphi_i - y\sin\varphi_i)}\hat{e}_z. \quad (5d)$$

The Poynting vector $\vec{S} = c_0/(8\pi)\cdot \mathrm{Re}\{\vec{E}\times\vec{H}^*\}$ of the incident field for both TM and TE mode can be calculated as follows:

$$\vec{S}^0 = \frac{c_0 n_m k_m^2}{8\pi}\left(\cos\varphi_i\hat{e}_x - \sin\varphi_i\hat{e}_y\right). \quad (6)$$

2.2. Solution of the potentials

By solving the wave equation (1) and considering the boundary conditions between different media the solution of the potentials can be obtained. The derivation of this solution for the scattering by multiple cylinders has been published elsewhere in detail [13]. The resulting formulas for the potentials are shortly summarized here and finally the near field solution will be presented.

The total field potentials outside the cylinders (u^t, v^t) can be written as

$$\begin{bmatrix} u^t(P) \\ v^t(P) \end{bmatrix} = \begin{bmatrix} u^0(P) \\ v^0(P) \end{bmatrix} + \begin{bmatrix} u^s(P) \\ v^s(P) \end{bmatrix}, \quad (7)$$

where (u^0, v^0) are the potentials of the incident field and (u^s, v^s) are the scattered field potentials. The incident field potentials can be expressed as

$$\begin{bmatrix} u^0(P) \\ v^0(P) \end{bmatrix} = \begin{bmatrix} \delta_{\mathrm{TM}} \\ 1-\delta_{\mathrm{TM}} \end{bmatrix} \sum_{n=-\infty}^{\infty} (-i)^n e^{in\phi} e^{in\varphi_i} \mathrm{J}_n(k_m\rho), \quad (8)$$

where J_n is the Bessel function of the first kind and $\delta_{\mathrm{TM}} = 1$ for a TM mode incident wave or $\delta_{\mathrm{TM}} = 0$ for a TE mode incident wave. The solution of the scattered field potentials is given by

$$\begin{bmatrix} u^s(P) \\ v^s(P) \end{bmatrix} = -\sum_{j=1}^{N}\sum_{n=-\infty}^{\infty} (-i)^n e^{in\gamma_{jP}} \mathrm{H}_n(k_m R_{jP}) \begin{bmatrix} b_{jn} \\ a_{jn} \end{bmatrix}, \quad (9)$$

where H_n corresponds to the Hankel function of the second kind. The expansion coefficients (a_{jn}, b_{jn}) are related to the single cylinder scattering coefficients (a^0_{jn}, b^0_{jn}) [1] and can be obtained by solving the following equation system [20]:

$$\sum_{l=1}^{N}\sum_{s=-\infty}^{\infty}\left(\delta_{lj}\delta_{ns}+(1-\delta_{lj})G^{jn}_{ls}\begin{bmatrix}b^0_{jn}\\ a^0_{jn}\end{bmatrix}\right)\begin{bmatrix}b_{ls}\\ a_{ls}\end{bmatrix}=\epsilon_j e^{in\varphi_i}\begin{bmatrix}b^0_{jn}\\ a^0_{jn}\end{bmatrix}, \tag{10}$$

$$G^{jn}_{ls}=(-i)^{s-n}\mathrm{H}_{s-n}(k_m R_{lj})e^{i(s-n)\gamma_{lj}}. \tag{11}$$

In the above expression δ denotes the Kronecker delta and $\epsilon_j=\exp(-ik_m(x_j\cos\varphi_i - y_j\sin\varphi_i))$ is the phase shift of the incident wave at the center point $\vec{P}_j=(x_j,y_j)$ of the jth cylinder relative to the origin O of the reference frame.

The total field potentials inside cylinder l (u^l, v^l), $l\in\{1\dots N\}$, can be expressed as

$$\begin{bmatrix}u^l(P)\\ v^l(P)\end{bmatrix}=\sum_{n=-\infty}^{\infty}(-i)^n e^{in\gamma_{lP}}\mathrm{J}_n(k_l R_{lP})\begin{bmatrix}B_{ln}\\ A_{ln}\end{bmatrix}. \tag{12}$$

The expansion coefficients for the internal fields (A_{ln}, B_{ln}) are related to the expansion coefficients of the scattered field (a_{jn}, b_{jn}) by

$$\begin{aligned}\begin{bmatrix}B_{ln}\\ A_{ln}\end{bmatrix}=&\left(\mathrm{J}_n(k_l a_l)\begin{bmatrix}m_l\\ m_l^2\end{bmatrix}\right)^{-1}\cdot\Bigg(\epsilon_l e^{in\varphi_i}\mathrm{J}_n(k_m a_l)-\begin{bmatrix}b_{ln}\\ a_{ln}\end{bmatrix}\mathrm{H}_n(k_m a_l)\\ &-\mathrm{J}_n(k_m a_l)\sum_{\substack{j=1\\ j\neq l}}^{N}\sum_{s=-\infty}^{\infty}(-i)^{s-n}\mathrm{H}_{s-n}(k_m R_{lj})e^{i(s-n)\gamma_{lj}}\begin{bmatrix}b_{js}\\ a_{js}\end{bmatrix}\Bigg).\end{aligned} \tag{13}$$

The solutions of the potentials can be inserted into equations (4) to get the near field solutions.

2.3. TM mode field solutions

For the TM mode the solution of the scattered field at any point P outside the cylinders is:

$$\begin{aligned}H^s_\rho=n_m\sum_{j=1}^{N}\sum_{n=-\infty}^{\infty}(-i)^n e^{in\gamma_{jP}}\Bigg(&\frac{in}{R_{jP}}\mathrm{H}_n(k_m R_{jP})\cos(\gamma_{jP}-\phi)\\ &+k_m\mathrm{H}'_n(k_m R_{jP})\sin(\gamma_{jP}-\phi)\Bigg)b_{jn},\end{aligned} \tag{14a}$$

$$\begin{aligned}H^s_\phi=n_m\sum_{j=1}^{N}\sum_{n=-\infty}^{\infty}(-i)^n e^{in\gamma_{jP}}\Bigg(&\frac{in}{R_{jP}}\mathrm{H}_n(k_m R_{jP})\sin(\gamma_{jP}-\phi)\\ &-k_m\mathrm{H}'_n(k_m R_{jP})\cos(\gamma_{jP}-\phi)\Bigg)b_{jn},\end{aligned} \tag{14b}$$

$$E^s_z=-ik_m\sum_{j=1}^{N}\sum_{n=-\infty}^{\infty}(-i)^n e^{in\gamma_{jP}}\mathrm{H}_n(k_m R_{jP})b_{jn}. \tag{14c}$$

In addition the solution for the total internal fields at any point P inside cylinder l can be obtained:

$$H_\rho^l = n_l \sum_{n=-\infty}^{\infty} (-i)^n e^{in\gamma_{lP}} \Bigg(-\frac{in}{R_{lP}} \mathrm{J}_n(k_l R_{lP}) \cos(\gamma_{lP} - \phi) - k_l \mathrm{J}_n'(k_l R_{lP}) \sin(\gamma_{lP} - \phi) \Bigg) B_{ln}, \tag{15a}$$

$$H_\phi^l = n_l \sum_{n=-\infty}^{\infty} (-i)^n e^{in\gamma_{lP}} \Bigg(-\frac{in}{R_{lP}} \mathrm{J}_n(k_l R_{lP}) \sin(\gamma_{lP} - \phi) + k_l \mathrm{J}_n'(k_l R_{lP}) \cos(\gamma_{lP} - \phi) \Bigg) B_{ln}, \tag{15b}$$

$$E_z^l = ik_l \sum_{n=-\infty}^{\infty} (-i)^n e^{in\gamma_{lP}} \mathrm{J}_n(k_l R_{lP}) B_{ln}. \tag{15c}$$

The solution of the time-averaged Poynting vector for the scattered field can be derived by using equations (14):

$$S_\rho^s = \frac{c_0 k_m n_m}{8\pi} \cdot \mathrm{Re} \Bigg\{ i \sum_{j=1}^{N} \sum_{n=-\infty}^{\infty} \sum_{l=1}^{N} \sum_{s=-\infty}^{\infty} (-i)^{n-s} e^{in\gamma_{jP} - is\gamma_{lP}} \Bigg(-\frac{is}{R_{lP}} \mathrm{H}_n(k_m R_{jP}) \mathrm{H}_s^*(k_m R_{lP}) \sin(\gamma_{lP} - \phi) - k_m \mathrm{H}_n(k_m R_{jP}) \mathrm{H}_s'^*(k_m R_{lP}) \cos(\gamma_{lP} - \phi) \Bigg) b_{jn} b_{ls}^* \Bigg\}, \tag{16a}$$

$$S_\phi^s = \frac{c_0 k_m n_m}{8\pi} \cdot \mathrm{Re} \Bigg\{ i \sum_{j=1}^{N} \sum_{n=-\infty}^{\infty} \sum_{l=1}^{N} \sum_{s=-\infty}^{\infty} (-i)^{n-s} e^{in\gamma_{jP} - is\gamma_{lP}} \Bigg(\frac{is}{R_{lP}} \mathrm{H}_n(k_m R_{jP}) \mathrm{H}_s^*(k_m R_{lP}) \cos(\gamma_{lP} - \phi) - k_m \mathrm{H}_n(k_m R_{jP}) \mathrm{H}_s'^*(k_m R_{lP}) \sin(\gamma_{lP} - \phi) \Bigg) b_{jn} b_{ls}^* \Bigg\}, \tag{16b}$$

$$S_z^s = 0. \tag{16c}$$

Also for the internal total fields inside cylinder l an expression for the Poynting vector can be derived from equations (15):

$$S_\rho^l = \frac{c_0 k_l n_l}{8\pi} \cdot \mathrm{Re}\Bigg\{ i \sum_{n=-\infty}^{\infty} \sum_{s=-\infty}^{\infty} (-i)^{n-s} e^{i(n-s)\gamma_{lP}} \Bigg(-\frac{is}{R_{lP}} \mathrm{J}_n(k_l R_{lP}) \mathrm{J}_s^*(k_l R_{lP}) \sin(\gamma_{lP} - \phi) - k_l \mathrm{J}_n(k_l R_{lP}) \mathrm{J}_s'^*(k_l R_{lP}) \cos(\gamma_{lP} - \phi) \Bigg) B_{ln} B_{ls}^* \Bigg\}, \tag{17a}$$

$$S_\phi^l = \frac{c_0 k_l n_l}{8\pi} \cdot \mathrm{Re}\Bigg\{ i \sum_{n=-\infty}^{\infty} \sum_{s=-\infty}^{\infty} (-i)^{n-s} e^{i(n-s)\gamma_{lP}} \Bigg(\frac{is}{R_{lP}} \mathrm{J}_n(k_l R_{lP}) \mathrm{J}_s^*(k_l R_{lP}) \cos(\gamma_{lP} - \phi) - k_l \mathrm{J}_n(k_l R_{lP}) \mathrm{J}_s'^*(k_l R_{lP}) \sin(\gamma_{lP} - \phi) \Bigg) B_{ln} B_{ls}^* \Bigg\}, \tag{17b}$$

$$S_z^l = 0. \tag{17c}$$

2.4. TE mode field solutions

The solution of the TE mode scattered field at any point P outside the cylinders is given by

$$E_\rho^s = \sum_{j=1}^{N} \sum_{n=-\infty}^{\infty} (-i)^n e^{in\gamma_{jP}} \Bigg(-\frac{in}{R_{jP}} \mathrm{H}_n(k_m R_{jP}) \cos(\gamma_{jP} - \phi) - k_m \mathrm{H}_n'(k_m R_{jP}) \sin(\gamma_{jP} - \phi) \Bigg) a_{jn}, \tag{18a}$$

$$E_\phi^s = \sum_{j=1}^{N} \sum_{n=-\infty}^{\infty} (-i)^n e^{in\gamma_{jP}} \Bigg(-\frac{in}{R_{jP}} \mathrm{H}_n(k_m R_{jP}) \sin(\gamma_{jP} - \phi) + k_m \mathrm{H}_n'(k_m R_{jP} \cos(\gamma_{jP} - \phi) \Bigg) a_{jn}, \tag{18b}$$

$$H_z^s = -ik_m n_m \sum_{j=1}^{N} \sum_{n=-\infty}^{\infty} (-i)^n e^{in\gamma_{jP}} \mathrm{H}_n(k_m R_{jP}) a_{jn}. \tag{18c}$$

The solution for the total internal fields at a point P inside cylinder l is:

$$E_\rho^l = \sum_{n=-\infty}^{\infty} (-i)^n e^{in\gamma_{lP}} \left(\frac{in}{R_{lP}} \mathrm{J}_n(k_l R_{lP}) \cos(\gamma_{lP} - \phi) + k_l \mathrm{J}_n'(k_l R_{lP}) \sin(\gamma_{lP} - \phi) \right) A_{ln}, \tag{19a}$$

$$E_\phi^l = \sum_{n=-\infty}^{\infty} (-i)^n e^{in\gamma_{lP}} \left(\frac{in}{R_{lP}} \mathrm{J}_n(k_l R_{lP}) \sin(\gamma_{lP} - \phi) - k_l \mathrm{J}_n'(k_l R_{lP}) \cos(\gamma_{lP} - \phi) \right) A_{ln}, \tag{19b}$$

$$H_z^l = ik_l n_l \sum_{n=-\infty}^{\infty} (-i)^n e^{in\gamma_{lP}} \mathrm{J}_n(k_l R_{lP}) A_{ln}. \tag{19c}$$

The time-averaged Poynting vector for the scattered field solution can be calculated as follows:

$$S_\rho^s = \frac{c_0 k_m n_m}{8\pi} \cdot \mathrm{Re}\Bigg\{ i \sum_{j=1}^{N} \sum_{n=-\infty}^{\infty} \sum_{l=1}^{N} \sum_{s=-\infty}^{\infty} (-i)^{n-s} e^{in\gamma_{jP} - is\gamma_{lP}} \left(-\frac{in}{R_{jP}} \mathrm{H}_n(k_m R_{jP}) \mathrm{H}_s^*(k_m R_{lP}) \sin(\gamma_{jP} - \phi) + k_m \mathrm{H}_n'(k_m R_{jP}) \mathrm{H}_s^*(k_m R_{lP}) \cos(\gamma_{jP} - \phi) \right) a_{jn} a_{ls}^* \Bigg\}, \tag{20a}$$

$$S_\phi^s = \frac{c_0 k_m n_m}{8\pi} \cdot \mathrm{Re}\Bigg\{ i \sum_{j=1}^{N} \sum_{n=-\infty}^{\infty} \sum_{l=1}^{N} \sum_{s=-\infty}^{\infty} (-i)^{n-s} e^{in\gamma_{jP} - is\gamma_{lP}} \left(\frac{in}{R_{jP}} \mathrm{H}_n(k_m R_{jP}) \mathrm{H}_s^*(k_m R_{lP}) \cos(\gamma_{jP} - \phi) + k_m \mathrm{H}_n'(k_m R_{jP}) \mathrm{H}_s^*(k_m R_{lP}) \sin(\gamma_{jP} - \phi) \right) a_{jn} a_{ls}^* \Bigg\}, \tag{20b}$$

$$S_z^s = 0. \tag{20c}$$

In addition the Poynting vector for the internal total fields inside cylinder l can be derived as

$$S_\rho^l = \frac{c_0 k_l n_l}{8\pi} \cdot \mathrm{Re}\Bigg\{ i \sum_{n=-\infty}^{\infty} \sum_{s=-\infty}^{\infty} (-i)^{n-s} e^{i(n-s)\gamma_{lP}} \Bigg(-\frac{in}{R_{lP}} \mathrm{J}_n(k_l R_{lP}) \mathrm{J}_s^*(k_l R_{lP}) \sin(\gamma_{lP} - \phi) + k_l \mathrm{J}_n'(k_l R_{lP}) \mathrm{J}_s^*(k_l R_{lP}) \cos(\gamma_{lP} - \phi) \Bigg) A_{ln} A_{ls}^* \Bigg\}, \tag{21a}$$

$$S_\phi^l = \frac{c_0 k_l n_l}{8\pi} \cdot \mathrm{Re}\Bigg\{ i \sum_{n=-\infty}^{\infty} \sum_{s=-\infty}^{\infty} (-i)^{n-s} e^{i(n-s)\gamma_{lP}} \Bigg(\frac{in}{R_{lP}} \mathrm{J}_n(k_l R_{lP}) \mathrm{J}_s^*(k_l R_{lP}) \cos(\gamma_{lP} - \phi) + k_l \mathrm{J}_n'(k_l R_{lP}) \mathrm{J}_s^*(k_l R_{lP}) \sin(\gamma_{lP} - \phi) \Bigg) A_{ln} A_{ls}^* \Bigg\}, \tag{21b}$$

$$S_z^l = 0. \tag{21c}$$

2.5. Total, scattered and incident fields

By definition the total field can be expressed as a sum of the scattered field and the incident field. Equations (14) and (18) are scattered field solutions while equations (15) and (19) are used to calculate the internal total fields. To get the total field solution from the scattered field equations or vice versa, the incident field which is given in Eqs. (5) has to be added or subtracted to the corresponding solution.

2.6. Normalization and scaling

For better comparison the results have been normalized by the incident field. This means, that each calculated field component (for both $\vec{E}$ and $\vec{H}$ fields) has been divided by the corresponding component of the incident electric field $\vec{E}^0$. This does not only provide a normalization of the field magnitudes, but also of the phases. The Poynting vector has been normalized by the corresponding Poynting vector of the incident field as well.

Finally, it should be noted that the system of units underlying the presented near field formulas is the cgs-system. However, the FDTD solution used in this work for validation purposes is based on the SI-system of units. In order to be able to compare absolute values the normalized magnetic fields calculated via the analytical solution have been additionally scaled by a factor of $(c_0\mu_0)^{-1}$, where c_0 is the speed of light in vacuum and μ_0 is the permeability of free space.

2.7. Cartesian coordinates

For the derivation of the multiple cylinder scattering solution the problem has been regarded in cylindrical coordinates. Also, the resulting near field vector components are

expressed in cylindrical coordinate basis. In order to get the solution vector in Cartesian coordinate basis the resulting vector components have to be transformed as follows:

$$\begin{pmatrix} F_x \\ F_y \\ F_z \end{pmatrix} = \begin{pmatrix} \cos\phi & -\sin\phi & 0 \\ \sin\phi & \cos\phi & 0 \\ 0 & 0 & 1 \end{pmatrix} \begin{pmatrix} F_\rho \\ F_\phi \\ F_z \end{pmatrix}. \tag{22}$$

3. Implementation and validation

For the calculation of equations (14) – (21) a MATLAB software package has been implemented which is available for download [21]. In this section implementation details as well as verification results are presented.

3.1. Truncation criterion

One difficulty in solving the above equations is the treatment of the infinite sums. A suitable truncation criterion has to be derived. This has been done for the single cylinder far field solution [1] and the same criterion has also been successfully used for the multiple cylinder far field solution [22]. Thereby the sum over n for a specific cylinder j has been evaluated for integer values between $n = -M_j \dots M_j$, where $M_j = \lceil (x_j + 4 \cdot \sqrt[3]{x_j} + 2) \rceil$ and $x_j = a_j k_j$ is the size parameter of cylinder j in the ensemble. For the near field solution it was found that the proposed truncation number is also applicable.

3.2. Verification of the near field results

In order to verify the results of the implemented software package different tests have been performed. At first, the implementation has been tested for the reproduction of the single cylinder scattering results. The near field solution for the scattering by a single cylinder has been formulated by Bohren and Huffman [1] and was also implemented into a MATLAB code [23]. With this program the validity of the multiple cylinder solution when regarding only a single scatterer could be proved. All field components could be identically reproduced with both implementations.

To be able to verify the near field results calculated for multiple cylinder scattering a FDTD simulation tool has been used. A detailed description of the FDTD tool can be found elsewhere [23]. The results of different comparison tests between both methods are presented below.

In a first test the near field results of all electric and magnetic field components have been compared directly. The scattering of a plane monochromatic wave ($\varphi_i = 0°$) with wavelength $\lambda = 600\,\mathrm{nm}$ by four randomly positioned dielectric cylinders with diameter $d = 0.5\,\mu\mathrm{m}$ and refractive index $n_{\mathrm{cyl}} = 1.33$ ($n_m = 1$) has been calculated using the analytical solution and the FDTD method. For the FDTD method a discretization size of $\Delta = \lambda/20$ has been used. The results for the magnitudes of the normalized electric and magnetic scattered TM and TE field components as well as the corresponding relative differences between the results of both methods are shown in figure 2. For a better scaling all relative errors above 50 percent are plotted in the same color. It can be seen that the relative error in regions with low scattered field magnitude is highest ($> 50\%$). This is due to the fact that in the FDTD method a steady error noise is present because of different numerical error sources [23] which distorts the results at low magnitude. Additionally,

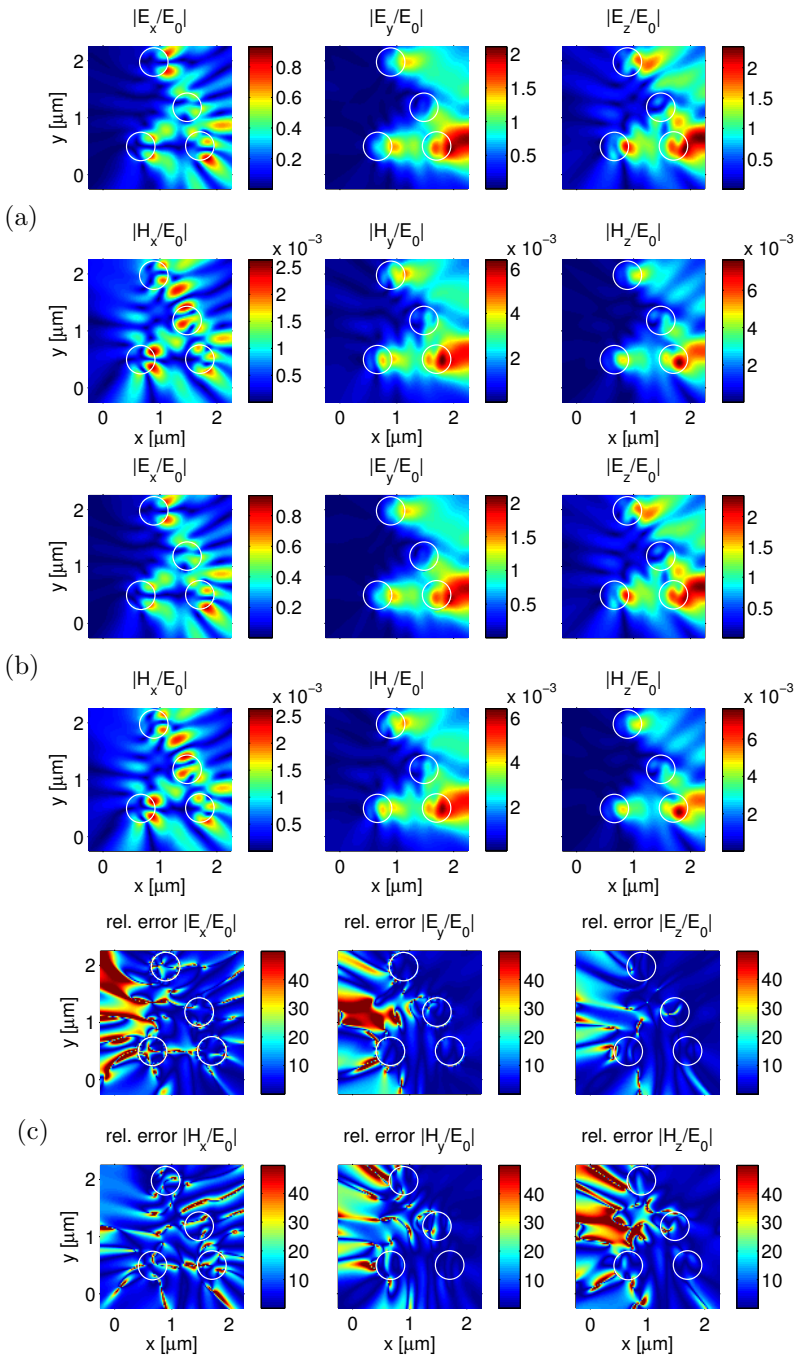

Figure 2: Near field magnitude for the scattering by four cylinders calculated with the (a) analytical solution and the (b) FDTD method. The relative difference between both methods is shown in (c). The cylinders are located at positions $(0.66, 0.49)$, $(1.7, 0.5)$, $(1.48, 1.18)$, $(0.89, 1.98)$ (in microns).

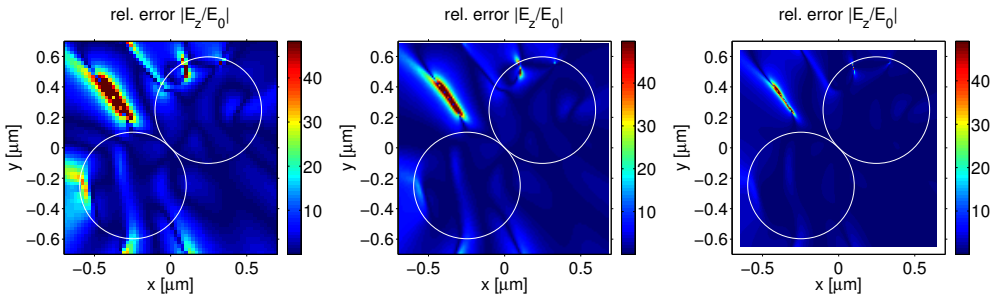

Figure 3: Convergence test for the scattering by two cylinders. The relative difference of the magnitude of the E_z component calculated with the FDTD method compared to the analytical solution is shown for $\Delta = \lambda/20$ (left), $\Delta = \lambda/40$ (middle) and $\Delta = \lambda/80$ (right).

in the FDTD method the field components are arranged in a staggered grid [18]. In the calculation of the analytical solution this arrangement has not been regarded, which means that the location where a certain field component has been evaluated is slightly shifted compared to the location of the corresponding component in the FDTD grid. Only the E_z component is evaluated at the same location in both methods, which in the end has been found to give the lowest error. However, for high magnitude fields the relative difference is less than 10 percent.

The differences observed in the previous test should result mainly from numerical errors inherent in the FDTD simulation while the analytical solution should give correct results. To verify this statement a convergence test has been performed. Under the assumption that the analytical solution is correct the FDTD solution should converge to the analytical solution as the discretization size in the FDTD method decreases. For this the scattering by two cylinders with diameter $d = 0.7\,\mu$m and refractive index $n_{\mathrm{cyl}} = 1.33$ has been regarded. The cylinder centers were separated by a full diameter (touching cylinders) and the connection line between the cylinder was set to form an angle of 45 degrees with the positive x-axis, which is the direction of the incident wave. The scattering of a plane TM wave ($\lambda = 600\,$nm, $n_m = 1$) by this two-particle system has been calculated with the FDTD method and compared to the analytical solution. For the convergence test the discretization size in the FDTD method has been altered from $\lambda/20$ to $\lambda/80$. The relative difference between the FDTD results and the analytical solution of the E_z component for three different discretization sizes ($\Delta = \lambda/20$, $\Delta = \lambda/40$ and $\Delta = \lambda/80$) are shown in figure 3. As expected a convergence behavior can be observed when the discretization size is scaled down.

In a last test the implementation has been validated for the calculation of the Poynting vector. There are two possibilities to calculate the Poynting vector. The first is to evaluate the electric and magnetic fields via equations (14), (15), (18) and (19) and get the Poynting vector by calculating the cross product of the fields afterward. The second way is to use equations (16), (17), (20) and (21) directly. It could be successfully verified that both methods give equal results. In addition, the results of the analytical solution have been compared to FDTD simulations. In figure 4 the Poynting vector for the scattering by two cylinders calculated by both methods is shown. The TM mode

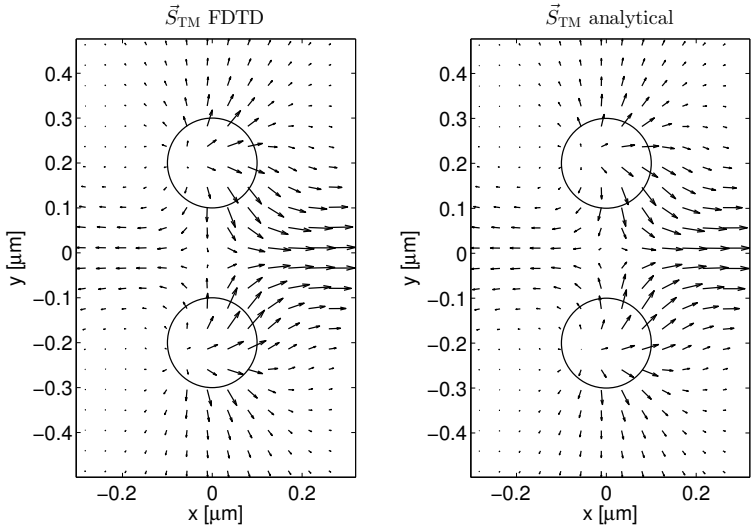

Figure 4: Poynting vector of the scattered fields for a TM incident field scattered by two cylinders. The shown results have been calculated with the FDTD (left) and the analytical method (right).

incident wave ($\varphi_i = 0°$) had a wavelength of $\lambda = 600\,\mathrm{nm}$, the cylinders had a diameter of $0.2\,\mu\mathrm{m}$ ($n_{\mathrm{cyl}} = 1.33$, $n_m = 1$) and were separated by $0.4\,\mu\mathrm{m}$. It can be seen that both methods can be used to reproduce similar results.

3.3. Computational complexity

In this section some remarks about the computational effort needed to solve the near field equations will be given. At first, to get the near field solution, the far field expansion coefficients have to be calculated. The difficulty thereby is the solution of the linear equation system (10). The size of this equation system is defined by the truncation numbers M_j and the total number of particles in the ensemble. The complexity to solve the problem increases quadratically with increasing number of particles or cylinder size. For the calculation of the near fields the effort increases only linearly with increasing size and number and additionally with the total number of near field locations to evaluate. In comparison the complexity of the 2D FDTD method is given by the total number of cells in the simulation grid which is determined by the problem size and the discretization length.

The FDTD method is advantageous compared to the analytical solution in means of computational speed for the calculation of the scattering by many densely packed cylinders confined in a volume small compared to the incident wavelength. Another advantage over the analytical solution is, that for non-dispersive materials the FDTD method offers the possibility to evaluate a whole spectral range in a single simulation [24] while with the analytical approach the problem would have to be solved multiple times. In the FDTD simulation considerable numerical errors are present and the discretization size has to be reduced to improve the accuracy. A discretization size of at least $\Delta = \lambda/20$ should be used to get acceptable results.

The analytical solution gives more accurate results than the FDTD solution. It is advantageous in calculating the scattering by a small number of particles, by widely separated particles or if just a small number of near field locations has to be evaluated. In the end the choice of the method has to be balanced between computational effort and gained accuracy.

4. Results

With the implemented near field solution for the scattering by multiple infinite cylinders some basic investigations have been performed which will be presented in this section.

4.1. Near to far field transition

At first, the near to far field transition has been examined numerically. In the scattered near fields surrounding the scatterer no clear direction of the energy flux can be specified. However, at distances far away from the scatterer the scattered field radiates as an outgoing cylindrical wave. This means the radial component of the scattered electric and magnetic fields vanishes and only the angular component is present. However, the direction of the energy flux, which is given by the Poynting vector, is radially aligned. So for the Poynting vector in contrary to the fields the angular component vanishes and only the radial component remains.

By using the analytical method to solve the near field solution the near to far field transition could be examined numerically by evaluating the scattered fields at increasing distances to the scattering center. For a certain scattering structure the Poynting vector has been calculated along a circle around the center of the structure for different circle radii. In addition, the far field scattering has been solved for the same scattering structure as reference. The Poynting vector has been normalized by a factor of $\rho k_m \pi/2$ in order to be comparable to the far field solution given in the form of amplitude scattering matrix elements [1].

In figure 5 the angular resolved Poynting vector components for the scattering of a TM mode wave ($\lambda = 600\,\mathrm{nm}$, $\varphi_i = 0°$, $n_m = 1$) by a single cylinder with diameter $d = 6\,\mu\mathrm{m}$ (radius $R = 3\,\mu\mathrm{m}$) and refractive index $n_{\mathrm{cyl}} = 1.33$ are shown. The Poynting vector has been calculated at different distances ρ around the cylinder center ($\rho/R \in \{2, 10, 100, 1000\}$). On the upper left-hand side the ρ component of the Poynting vector of the near field solution is plotted together with the far field solution. On the upper right the ϕ component is shown which vanishes in the far field. In the bottom left figure the relative difference between the near field results for $\rho/R \in \{100, 1000\}$ and the far field solution is presented. On the right-hand side the value of the ϕ component normalized by the ρ component of the far field solution is plotted. It can be seen that as the distance to the center increases the near field solution converges to the far field solution. A deviation of less than 30 percent for $\rho/R = 100$ and less than 3 percent for $\rho/R = 1000$ is observed for the ρ components. As expected, the ϕ component of the near field solution approaches zero as the distance to the center increases. The same investigation has been performed for a structure consisting of many cylinders. Five cylinders with diameter $d = 2\,\mu\mathrm{m}$ have been placed in a $6\,\mu\mathrm{m}$ circle as is shown in the inlay of figure 6. The same parameters for the refractive indices and the incident wavelength have been used as before. The scattering has been calculated for the same distances as above, the results

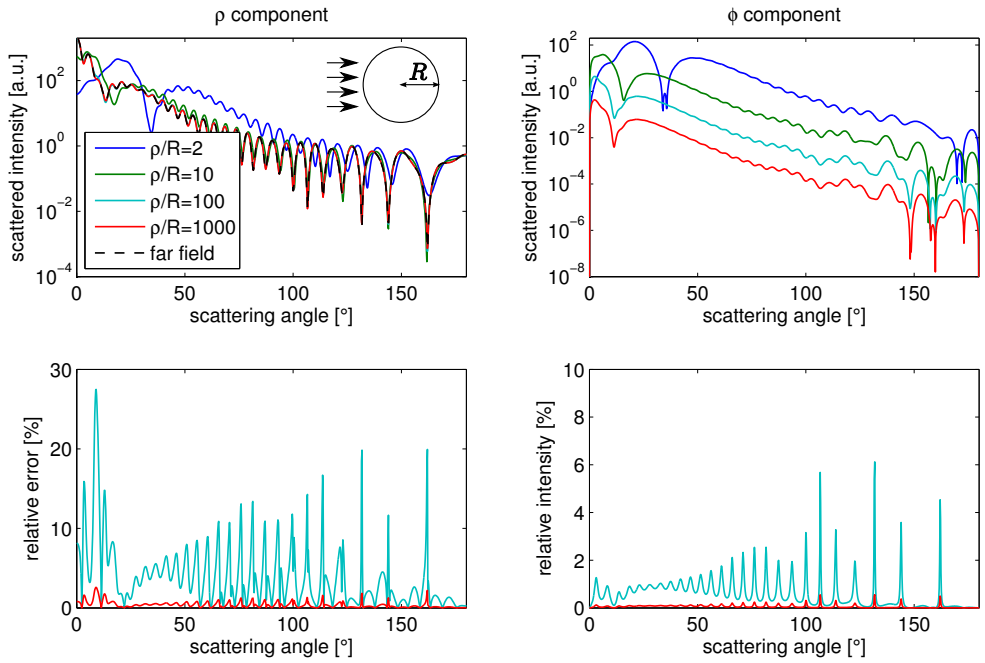

Figure 5: Comparison of the angular resolved far field solution with near field results for a single cylinder at various distances to the scatterer center.

of the components of the Poynting vector are shown in the figure. It can be seen that the near field results converge to the far field solution. However, the relative differences are larger than for the single cylinder case. This is interesting to see, because the radius of the circle where the scatterers are confined stays the same as before. Obviously, due to the near field interaction of the cylinders in the ensemble the fields converge slower to the far field solution.

In principle the approach shown here could be used to systematically investigate the near to far field transition for scatterers of various sizes and compositions. However, the task of doing such a thorough analysis has not been part of this paper's work.

4.2. Photonic nanojets

In a further investigation the analytical approach has been used to examine photonic nanojets and the focussing of light through multiple cylindrical particles. A photonic nanojet is a local enhancement of the total field intensity which can be observed behind a spherical or cylindrical scatterer [25, 16]. The formation of a nanojet can be seen as a small dimension equivalent to the focussing of a spherical or cylindrical lens which is known from geometrical optics [23].

It was shown that the energy of a photonic nanojet can be transported through a chain of spherical particles [26]. In this article the transport of the nanojet energy through a multiparticle cylindrical system is investigated. The formation of the nanojet behind a single cylindrical particle can be seen in the upper left graph in figure 7. The cylinder

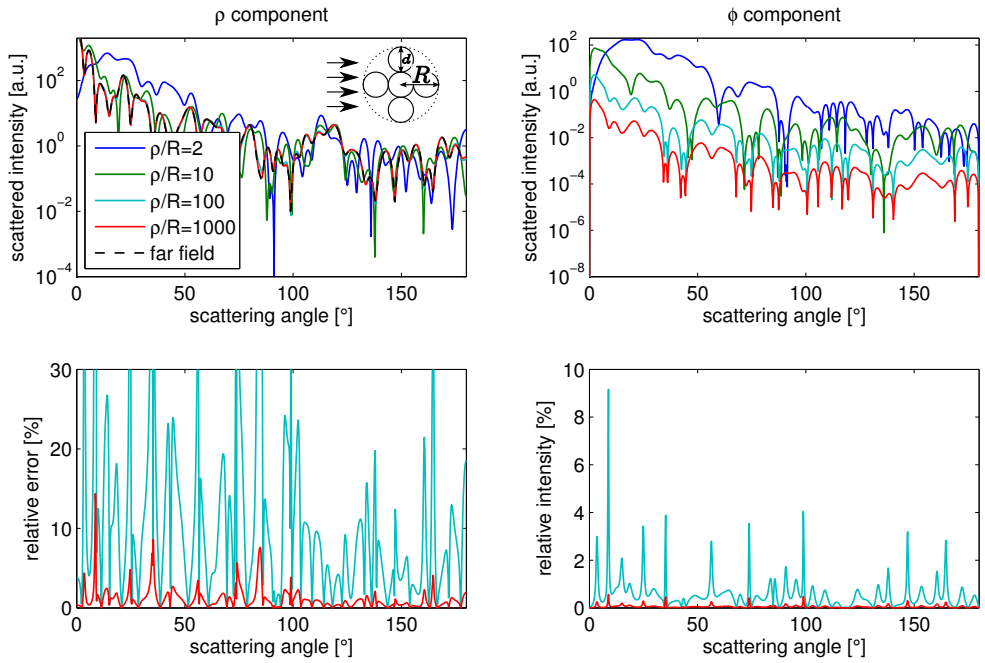

Figure 6: Comparison of the angular resolved far field solution with near field results for the scattering by five cylinders at various distances to the center of the scattering system.

was 6 μm in diameter with refractive index $n_{\mathrm{cyl}} = 1.33$ ($n_m = 1$). The total field solution has been calculated for an incident TM mode wave with a wavelength of $\lambda = 600\,\mathrm{nm}$ ($\varphi_i = 0°$). At the right-hand side the intensity along the x-axis for $y = 0$ is shown. The nanojet peak can clearly be observed behind the particle. By placing a second particle at a distance of 12 μm behind the first particle the intensity of the first peak stays the same and a little amount of light is focussed along the forward direction, which can be seen in the center graphs of figure 7. By placing a third particle 12 μm behind the second one another peak occurs in the intensity image as can be seen in the graphs at the bottom. The light which is slightly focussed by the second cylinder is focussed again by the third cylinder which produces a second peak about half the intensity of the first one. In principle such a multiparticle system can be seen as a small dimension equivalent of a lens system.

The calculations shown in this section give a short overview of the possibilities for the usage of the presented near field solution. Some interesting phenomena like local field enhancements can only be investigated by looking at the near field results.

5. Conclusion

In this paper the near field solution for the scattering of a plane electromagnetic wave by multiple infinite parallel cylinders at perpendicular incidence has been presented. An

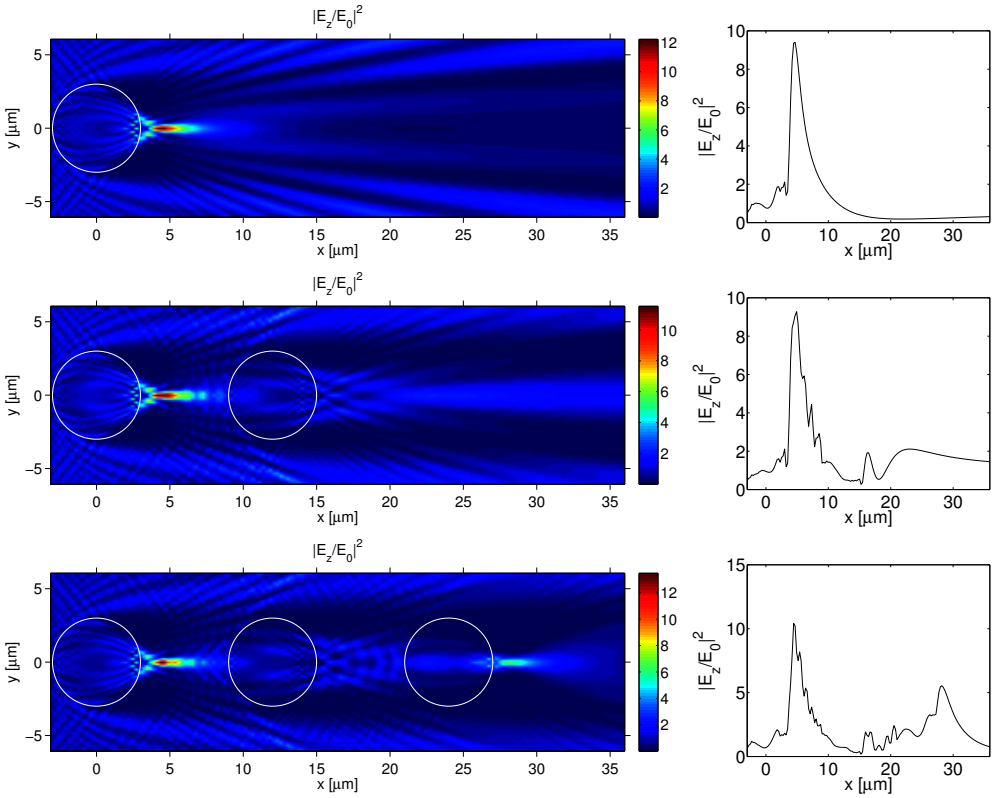

Figure 7: Formation and energy transport of a photonic nanojet by multiple cylindrical scatterers.

implementation of the solution of these formulas was developed and has been made available for download [21]. This implementation was successfully validated by comparing the results to FDTD simulations. To provide some examples of applicability the implemented tool has been used to examine the near to far field transition for the scattering by multiple cylinders and to visualize the transport of the energy of a photonic nanojet through a multiparticle system.

6. Acknowledgement

We acknowledge support of the Deutsche Forschungsgemeinschaft.

7. Bibliography

References

[1] Bohren CF, Huffman DR. Absorption and scattering of light by small particles. New York: Wiley-Interscience; 1998.

[2] Gurjar RS, Backman V, Perelman LT, Georgakoudi I, Badizadegan K, Itzkan I, et al. Imaging human epithelial properties with polarized light-scattering spectroscopy. Nat Med 2001;7(11):1245–8.
[3] Liu L, Mishchenko MI, Arnott WP. A study of radiative properties of fractal soot aggregates using the superposition T-matrix method. J Quant Spectrosc Radiat Transfer 2008;109(15):2656–63.
[4] Mie G. Beiträge zur Optik trüber Medien, speziell kolloidaler Metallösungen. Ann Phys 1908;330(3):377–445.
[5] Kerker M. The scattering of light and other electromagnetic radiation. New York: Academic Press; 1969.
[6] Xu YL. Electromagnetic scattering by an aggregate of spheres. Appl Opt 1995;34(21):4573–88.
[7] Gouesbet G, Gréhan G. Generalized Lorenz-Mie theories. Berlin: Springer; 2011.
[8] Lee SC. A quasidependent scattering radiative properties model for high density fiber composites. J Heat Transfer 2010;132(2).
[9] Kienle A, Hibst R. Light guiding in biological tissue due to scattering. Phys Rev Lett 2006;97(1).
[10] Wang RT, van de Hulst HC. Application of the exact solution for scattering by an infinite cylinder to the estimation of scattering by a finite cylinder. Appl Opt 1995;34(15):2811–21.
[11] Barabas M. Scattering of a plane wave by a radially stratified tilted cylinder. J Opt Soc Am A 1987;4(12):2240–8.
[12] Yousif HA, Köhler S. A Fortran code for the scattering of EM plane waves by two cylinders at normal incidence. Comp Phys Comm 1990;59(2):371–86.
[13] Lee SC. Dependent scattering of an obliquely incident plane wave by a collection of parallel cylinders. J Appl Phys 1990;68(10):4952–7.
[14] Elsherbeni AZ, Kishk AA. Modeling of cylindrical objects by circular dielectric and conducting cylinders. IEEE Trans Antennas Propag 1992;40(1):96–9.
[15] Kozaki S. Scattering of a gaussian beam by a homogeneous dielectric cylinder. J Appl Phys 1982;53(11):7195–200.
[16] Li X, Chen Z, Taflove A, Backman V. Optical analysis of nanoparticles via enhanced backscattering facilitated by 3-D photonic nanojets. Opt Express 2005;13(2):526–33.
[17] Hao E, Schatz GC. Electromagnetic fields around silver nanoparticles and dimers. J Chem Phys 2004;120(1):357–66.
[18] Taflove A, Hagness SC. Computational electrodynamics: The finite difference time-domain method. Boston: Artech House; 2005.
[19] Henin BH, Elsherbeni AZ, Sharkawy MA. Oblique incidence plane wave scattering from an array of circular dielectric cylinders. Progress In Electromagnetics Research, PIER 2007;68:261–179.
[20] Lee SC. Scattering by closely-spaced radially-stratified parallel cylinders. J Quant Spectrosc Radiat Transfer 1992;48(2):119–30.
[21] Schäfer J. MatScat. http://www.mathworks.com/matlabcentral/fileexchange/36831.
[22] Schäfer J, Kienle A. Scattering of light by multiple dielectric cylinders: comparison of radiative transfer and Maxwell theory. Opt Lett 2008;33(20):2413–5.
[23] Schäfer JP. Implementierung und Anwendung analytischer und numerischer Verfahren zur Lösung der Maxwellgleichungen für die Untersuchung der Lichtausbreitung in biologischem Gewebe. Ph.D. thesis; Universität Ulm; 2011.
[24] Drezek R, Dunn A, Richards-Kortum R. A pulsed finite-difference time-domain (FDTD) method for calculating light scattering from biological cells over broad wavelength ranges. Opt Express 2000;6(7):147–57.
[25] Chen Z, Taflove A, Backman V. Photonic nanojet enhancement of backscattering of light by nanoparticles: a potential novel visible-light ultramicroscopy technique. Opt Express 2004;12(7):1214–20.
[26] Chen Z, Taflove A, Backman V. Highly efficient optical coupling and transport phenomena in chains of dielectric microspheres. Opt Lett 2006;31(3):389–91.